Acta Crystallographica Section D
Biological Crystallography
ISSN 0907-4449

Structures of OppA and PstS from *Yersinia pestis* indicate variability of interactions with transmembrane domains

Mikio Tanabe,[a,b] Osman Mirza,[a] Thomas Bertrand,[b] Helen S. Atkins,[c] Richard W. Titball,[c] So Iwata,[a] Katherine A. Brown[b]* and Bernadette Byrne[a]

[a]Membrane Protein Crystallography, Division of Molecular Biosciences, Imperial College London, London SW7 2AZ, England, [b]Centre for Molecular Microbiology and Infection, Division of Cell and Molecular Biology, Imperial College London, London SW7 2AZ, England, and [c]Defence Science and Technology Laboratories, Porton Down, Salisbury SP4 0JQ, England

Correspondence e-mail: k.brown@imperial.ac.uk

Received 31 May 2007
Accepted 2 October 2007

PDB References: PstS, 2z22, r2z22sf; OppA, 2z23, r2z23sf.

Bacterial ATP-binding cassette (ABC) transport systems couple ATP hydrolysis with the uptake and efflux of a wide range of substances across bacterial membranes. These systems are comprised of transmembrane domains, nucleotide binding domains and, in the case of uptake systems, periplasmic binding proteins responsible for binding and presentation of substrate to the transmembrane domains. In pathogenic bacteria, ABC systems are known to play roles in virulence and pathogenicity and the surface localization of some components has made them attractive targets for both vaccine and anti-infective development. Here, the crystallization of five proteins (OppA, PstS, PiuA, YrbD and CysP) from *Yersinia pestis*, the causative agent of plague, are reported that diffracted to resolution limits ranging from 1.6 to 5 Å. The first crystal structures of ABC system components from *Y. pestis*, OppA and PstS, are also reported here as complexes with their substrates. Comparisons of these two structures with known structures of related proteins suggest that these proteins possess versatility in substrate recognition and variations in protein–protein interactions with their cognate transmembrane domains.

1. Introduction

ATP-binding cassette (ABC) transport systems comprise one of the largest membrane-protein families, being responsible for the transport of a diverse range of molecules across membranes. ABC transporters have two transmembrane domains (TMDs) and two ATP-binding or nucleotide-binding domains (NBDs). In Gram-negative bacteria, periplasmic binding proteins (PBP) are present that mediate the transport of specific substrates from the outer membrane to the inner membrane, where the TMDs are located (Higgins, 1992). Several high-resolution crystal structures of complete bacterial ABC transporters have been determined: the vitamin B_{12} transporter BtuCD (Locher *et al.*, 2002), the multidrug ABC transporter Sav1866 (Dawson & Locher, 2006), the metal-chelate-type ABC transporter HI1470/1 (Pinkett *et al.*, 2007) and the $ModB_2C_2$ transporter in complex with its binding protein ModA (Hollenstein *et al.*, 2007). The structures have helped to establish how these multisubunit complexes are assembled and have provided insights into ABC transport mechanisms.

Bacterial ABC transporters have a wide range of physiological roles that enable survival in diverse environments. Broadly, these systems can be divided into importers or uptake systems and exporters or efflux systems (reviewed by

Davidson & Chen, 2004), although ABC transporters with nontransport functions exist, such as those for DNA repair (Goosen & Moolenaar, 2001) or lipid biogenesis (Yakushi *et al.*, 2000). Importers are often involved in the uptake of nutrients such as sugars (Schneider, 2001), metal ions and complexes (Hantke, 2005; Koster, 2005) and peptides (Detmers *et al.*, 2001), and are therefore important in bacterial metabolism and survival. In comparison, exporters can play roles in bacterial virulence and pathogenicity, exemplified by efflux systems associated with multidrug resistance or the export of pore-forming toxin degradative enzymes (reviewed by Piddock, 2006). In addition, because some ABC system components are associated with virulence or survival in the host, are located at or near the bacterial cell surface, lack homologues in mammalian systems and can provide protective immunity, this class of proteins is a potential target for antimicrobial and vaccine development (Garmory & Titball, 2004).

Yersinia pestis, the causative agent of plague, is transmitted to humans *via* bites from rodents and their associated fleas. There are three forms of plague: bubonic, septicaemic and pneumonic plague. In the pneumonic form, *Y. pestis* can be transmitted person to person or animal to person *via* inhalation of contaminated air droplets (Perry & Fetherston, 1997). This mode of transmission has led to the identification of *Y. pestis* as a potential biological weapon (Inglesby *et al.*, 2002). As part of an effort to develop new vaccines against plague, we are pursuing a programme of X-ray studies of ABC transport proteins, which have been identified as candidate antigens using the genome sequence of *Y. pestis* (Parkhill *et al.*, 2001). Here, we report the crystallization of five different putative *Y. pestis* ABC transporter proteins or PBPs. We also report the first crystal structures of two PBPs from *Y. pestis*: OppA, part of the oligopeptide transporter system protein, which we have recently shown is a protective antigen against plague (Tanabe *et al.*, 2006), and PstS, part of a phosphate transporter system. Comparative structural analysis of their active sites suggests that both proteins have the ability to transport multiple peptides or phosphate compounds and this versatility in the substrate-binding sites may contribute to the survival of *Y. pestis* in its different environmental niches. In addition, examination of their surfaces suggests that the nature of the interactions of between PBPs and TMDs could in some cases be dominated by non-electrostatic forces.

2. Materials and methods

2.1. Protein expression and purification

Y. pestis DNA and protein sequences corresponding to each target were obtained from the Wellcome Trust *Y. pestis* genome database (Parkhill *et al.*, 2001). Oligonucleotides were designed incorporating a 5′ *Eco*RI or *Sal*I site and a 3′ *Xho*I site. OppA and PstS were expressed as the full-length proteins including signal sequences, while CysP (residues 36–345) and YrbD (residues 27–185) were expressed as truncated forms lacking the transmembrane domains as predicted by *TMHMM* (Krogh *et al.*, 2001). PiuA (residues 21–321) was expressed as a truncate corresponding to those regions of the protein found to be antigenic in studies with *Streptococcus pneumoniae* PiuA (Brown *et al.*, 2001). The resultant gene products were cloned into either pET28a(+) or pET24a(+) (CN Biosciences) expression vectors incorporating an N-terminal or C-terminal six-histidine tag, respectively. The cloned genes were transformed into *Escherichia coli* BL21 (DE3) cells. The cells were grown in LB medium and protein expression was induced with 0.2 m*M* IPTG for 6 h at 293 K (PiuA-pET28) or 0.5 m*M* IPTG for 4 h at 310 K (PstS-pET24, OppA-pET24, YrbD-pET28 and CysP-pET28). CysP, PiuA and YrbD were expressed in the cytoplasm, while OppA and PstS were expressed in the periplasm.

The basic protein-purification protocol was adapted from previously published methods (Sambrook & Russell, 2001). All procedures were carried out at 277 K. *E. coli* cells expressing individual target proteins were incubated with 1% lysozyme in treatment buffer (200 m*M* Tris–HCl pH 8.8, 20 m*M* Na EDTA, 500 m*M* sucrose) for 30 min. The periplasmic fraction was separated by centrifugation at 12 000*g* for 15 min. The supernatant was isolated and used for purification in the case of PstS. In the cases of CysP, PiuA and YrbD, the remaining cells were disrupted by sonication using a VCX500 sonicator (Sonics and Material Inc.) for 2 × 5 min bursts in cell-disruption buffer (5 m*M* Na EDTA, 1 µg ml^{-1} DNaseI, 0.5 m*M* PMSF). The sample was centrifuged at 10 000*g* for 15 min to remove debris. The supernatant containing the expressed proteins was separated from the insoluble fraction by centrifugation at 100 000*g* for 1.5 h. For OppA, the periplasmic fraction was obtained by osmotic shock using a previously published method (Guyer *et al.*, 1985). Na EDTA and low-molecular-weight proteins in the soluble fractions were removed by filtration through a 10 kDa molecular-weight cutoff filter (Millipore) prior to incubation with Ni^{2+} resin.

The concentrated protein solutions were incubated with Ni^{2+} resin equilibrated with buffer *A* (50 m*M* Tris–HCl pH 7.5, 100 m*M* NaCl, 5 m*M* imidazole) for 2 h at 277 K. After extensive washing of the resin, proteins were eluted with buffer *A* containing 100 m*M* imidazole.

Protein concentration was determined using the Bradford method (Bio-Rad) or using a BCA kit (Pierce/Perbio Science). Bovine serum albumin (BSA) was used as a protein standard.

2.2. Protein crystallization and data collection

Initial crystallization trials were set up by a crystallization robot (Cartesian) in 96-well plates using the sitting-drop vapour-diffusion method. The screening solutions were obtained from Hampton Research, Molecular Dimensions Ltd and an in-house screening kit. The robot dispenses drops consisting of 0.2 µl protein solution at various concentrations plus 0.2 µl reservoir solution. The drops were equilibrated against 200 µl reservoir solution at 277 and 293 K. All protein crystals described here were obtained using this initial screening process. For optimization, drops consisting of 1 µl

protein solution plus 1 µl reservoir solution were incubated with 800 µl reservoir solution using the hanging-drop vapour-diffusion method.

For OppA, 20 mg purified protein (in 2 ml 10 m*M* HEPES–NaOH pH 7.5) was incubated with 100 mg trilysine peptide (in 10 ml 10 m*M* HEPES–NaOH pH 7.5) overnight at 277 K. Prior to the setting up of initial crystallization trials, the OppA–trilysine complex was concentrated to 20 mg ml^{-1} in 10 m*M* HEPES–NaOH pH 7.5. Initial crystals were grown in 30%(*w*/*v*) PEG 1500 using the sitting-drop method. For optimization, OppA protein (∼50 mg ml^{-1} in 10 m*M* HEPES–NaOH pH 7.5) was mixed with a reservoir solution consisting of 32%(*w*/*v*) PEG 1500 and 3% aminocaproic acid in a 1:1 ratio. Crystals grew to maximum dimensions of 100 × 50 × 300 µm within 3 d at 293 K. Crystals intended for X-ray data collection were soaked in vitrification solutions with an increasing concentration of PEG 1500 (to 35%) and 10%(*v*/*v*) methyl-2,4-pentanediol (MPD) and flash-frozen in liquid nitrogen.

For PstS, purified protein was concentrated to 15 mg ml^{-1} in 10 m*M* Tris–HCl pH 7.2. PstS crystals were first obtained in 100 m*M* HEPES–NaOH pH 7.5, 20%(*w*/*v*) PEG 10 000. For optimization, PstS protein (∼15 mg ml^{-1} in 10 m*M* Tris–HCl pH 7.2) was mixed in a 1:1 ratio with reservoir consisting of

Table 1
Data-collection statistics.

Values in parentheses are for the highest resolution shell.

	OppA	PstS	PiuA	YrbD
Space group	$P2_12_12_1$	$P2_1$	$P422$	$P6_1$ or $P6_5$
Unit-cell parameters				
a (Å)	71.82	68.93	50.15	137.65
b (Å)	90.63	60.82	50.15	137.65
c (Å)	93.70	78.78	196.24	109.68
α (°)	90	90	90	90
β (°)	900	100.14	90	120
γ (°)	90	90	90	90
Synchrotron source	ESRF ID29	SRS14.1	ESRF ID29	SRS14.1
No. of molecules per ASU	1	2	1	4–8
Resolution range (Å)	30–1.8 (1.85–1.8)	30–2.0 (2.06–2.0)	30–2.9 (2.99–2.9)	30–3.2 (3.29–3.2)
No. of unique reflections	71053	42809	6131	26091
Angular increment per frame (°)	1	1	1	1
Rotation range (°)	180	180	150	180
Completeness	87.4 (88.1)	97.8 (94.7)	97.7 (100)	99.2 (100)
$R_{\rm sym}$†	0.080 (0.587)	0.080 (0.134)	0.105 (0.514)	0.104 (0.560)
$I/\sigma(I)$	12.9 (1.9)	18.06 (11.2)	11.3 (4.4)	17.5 (4.3)
Wilson B factor (Å^2)	34.1	21.0		

† $R_{\rm sym} = \sum_h \sum_i |I_{hi} - I_h| / \sum_h \sum_i I_h$, where I_h is the mean intensity of the reflection.

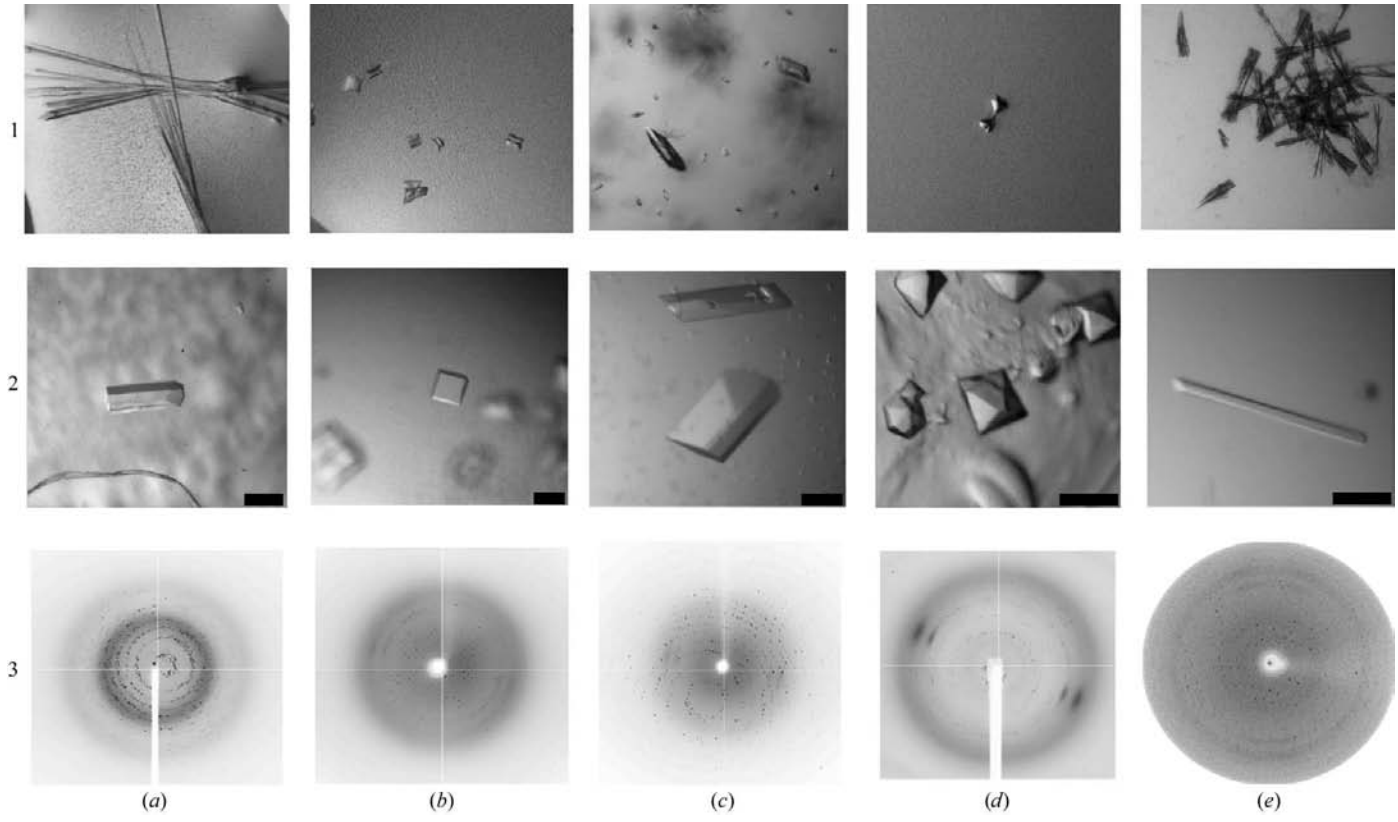

Figure 1
Crystals and diffraction images for the crystallized target proteins. Rows 1, 2 and 3 show the initial crystals obtained from 96-well plate preliminary screens, optimized crystals and a typical diffraction image, respectively. It was possible to obtain diffracting crystals of (*a*) OppA, (*b*) PstS, (*c*) PiuA, (*d*) YrbD and (*e*) CysP with diffraction limits of 1.6, 2.0, 2.8, 2.8 and 5.0 Å, respectively. The scale bars shown on the figures in row 2 represent 100 µm.

100 m*M* HEPES–NaOH pH 7.5, 22%(*w*/*v*) PEG 10 000 and 10 m*M* $MgCl_2$. After optimization, crystals grew to maximum dimensions of 200 × 250 × 150 µm within 48 h at 293 K. Crystals were vitrified in 25%(*w*/*v*) PEG 10 000 and 10%(*v*/*v*) MPD or 20%(*v*/*v*) glycerol.

For PiuA, purified protein was concentrated to 20 mg ml^{-1} in 10 m*M* HEPES–NaOH pH 7.5. Initial crystals were observed in 30%(*w*/*v*) PEG 1500 in sitting drops. For optimization, PiuA protein (~20 mg ml^{-1} in 10 m*M* HEPES–NaOH pH 7.5) was mixed in a 1:1 ratio with reservoir consisting of 30%(*w*/*v*) PEG 1500 and 1 m*M* $BaCl_2$. Crystals grew to maximum dimensions of 200 × 200 × 50 µm within 48 h at 293 K. Crystals were vitrified using a reservoir solution adjusted to 35%(*w*/*v*) PEG 1500 with 10%(*v*/*v*) MPD.

For YrbD, purified protein was concentrated to 40 mg ml^{-1} in 10 m*M* HEPES–NaOH pH 7.5. Initial crystals of YrbD were grown in 100 m*M* CHES pH 9.5, 30%(*w*/*v*) PEG 400, 100 m*M* NaCl and 100 m*M* $MgCl_2$ in sitting drops. For optimization, YrbD protein (~50 mg ml^{-1} in 10 m*M* HEPES–NaOH) was mixed in a 1:1 ratio with reservoir consisting of 20 m*M* EDTA pH 8.0, 28%(*w*/*v*) PEG 400, 100 m*M* NaCl and $MgCl_2$. Crystals grew to maximum dimensions of 150 × 100 × 100 µm in around 2–3 weeks. Crystals were vitrified in liquid N_2 before data collection in the presence of an increased PEG 400 concentration [30–32%(*w*/*v*)].

For CysP, purified protein was buffer-exchanged into 10 m*M* HEPES–NaOH pH 7.5. Initial crystals were obtained in 200 m*M* ammonium sulfate, 100 m*M* sodium acetate trihydrate pH 4.6 and 30%(*w*/*v*) PEG 4000 at 293 K. Optimization was performed using 24-well hanging drops containing 0.9 µl CysP (20 mg ml^{-1} in 10 m*M* HEPES–NaOH pH 7.5) mixed with 0.9 µl reservoir solution consisting of 200 m*M* ammonium sulfate, 10 m*M* Li_2SO_4, 100 m*M* sodium acetate trihydrate pH 5.0 and 28%(*w*/*v*) PEG 4000. Crystals were vitrified in liquid N_2 in the presence of 30%(*w*/*v*) PEG 4000 and 20%(*v*/*v*) glycerol prior to data collection.

OppA and YrbD data sets were collected at the ESRF (European Synchrotron Radiation Facility) beamline ID29 using an ADSC Quantum 4 CCD detector. PstS and PiuA data sets were collected at the Daresbury Synchrotron Radiation Source (SRS, Daresbury, Warrington, England) beamline 14.1 using an ADSC Quantum 4 CCD detector. All data were collected from crystals vitrified at 100 K. All data sets were processed using *DENZO*/*SCALEPACK* (Otwinowski & Minor, 1997). Images from

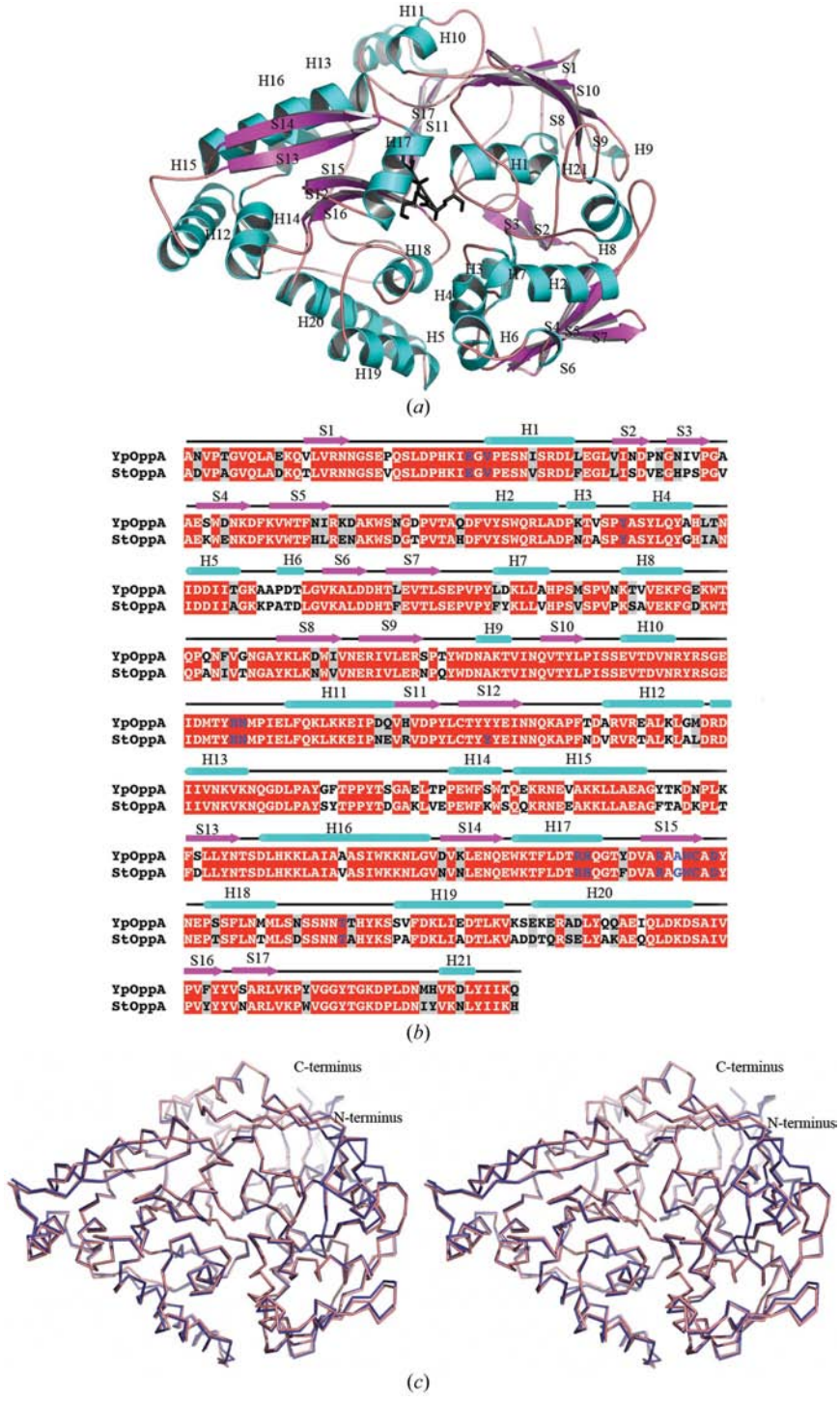

Figure 2
(*a*) Ribbon representation of *Y. pestis* OppA. β-Strands are labelled S1–S17 (purple) and helices are labelled H1–H21 (light blue). The trilysine substrate is represented by a stick model. (*b*) The sequences of *Y. pestis* OppA (YpOppA) and *S. typhimurium* OppA (StOppA) aligned using *CLUSTALW* (Thompson *et al.*, 1994). Strands and helices are indicated by purple arrows and light-blue cylinders, respectively. Conserved residues, nonconserved residues and the residues involved in substrate binding are shown in white, black and blue, respectively. (*c*) Parallel stereoview of the superposition of the *Y. pestis* OppA (pink) and the *S. typhimurium* OppA (dark blue) structures.

Table 2
PstS and OppA data-refinement statistics.

Values in parentheses are for the highest resolution shell.

	OppA	PstS
Resolution range (Å)	30–2.0 (2.03–2.0)	30–2.0 (2.02–2.0)
No. of molecules per ASU	1	2
No. of protein atoms	517	642
No. of water molecules	414	484
R_{work}† (%)	21.0 (35.8)	17.9 (21.6)
R_{free}‡ (%)	23.9 (38.0)	21.6 (27.3)
R.m.s.d. bond lengths (Å)	0.0078	0.0049
R.m.s.d. bond angles (°)	1.80	1.27
Ramachandran plot		
Most favourable regions (%)	88.7	93.1
Additional allowed regions (%)	11.3	6.9

† $R_{work} = \sum ||F_o| - |F_c|| / \sum |F_o|$. ‡ R_{free} is the R value for a 10% subset of randomly selected reflection data which were excluded from refinement.

the CysP crystals were collected using a Rigaku/MSC 3U300 X-ray generator with a MAR345 detector.

2.3. Structure solution and refinement

The OppA structure was solved by the molecular-replacement method using the coordinates of *Salmonella enterica* serovar Typhimurium (*S. typhimurium*) OppA (PDB code 2olb; Tame *et al.*, 1995) as a search model in *Phaser* (Storoni *et al.*, 2004) as implemented in the *CCP*4 suite (Collaborative Computational Project, Number 4, 1994). The PstS structure was solved by molecular replacement using the coordinates of the *E. coli* phosphate-binding protein (PBP; PDB code 2abh; Luecke & Quiocho, 1990) as a search model in *MOLREP* (Vagin & Teplyakov, 2000) in the *CCP*4 suite. For both structures, density modification and crystallographic refinement procedures were carried out using *ARP*/*wARP* (Lamzin *et al.*, 2001), *REFMAC*5 (Murshudov *et al.*, 1997) and *CNS* (Brünger *et al.*, 1998). Model building was performed using the program *O* (Jones *et al.*, 1991).

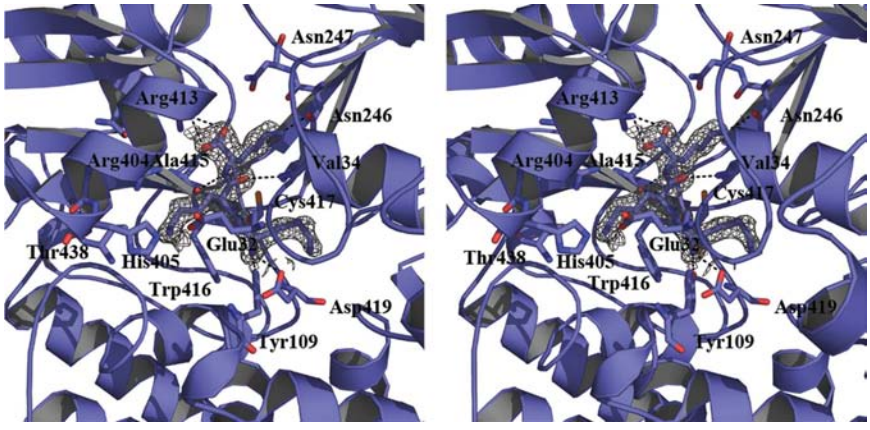

Figure 3
Substrate-binding site of *Y. pestis* OppA shown in parallel stereo. Key binding-site residues are labelled. Electron density for the trilysine molecule is shown generated from a $2F_o - F_c$ difference electron-density map contoured at 1σ. Hydrogen bonds between OppA and trilysine are shown as dotted lines.

2.4. Analysis of sequence and structure and validation

The *Y. pestis* OppA and PstS structures were validated using the program *PROCHECK* (Laskowski *et al.*, 1993). Amino-acid sequence alignments of the bacterial OppA and PstS sequences were performed using the program *CLUSTALW* (Thompson *et al.*, 1994). Structural alignments and superpositions of the *Y. pestis* OppA structure with the *S. typhimurium* OppA structure and of the *Y. pestis* PstS structure with the *E. coli* PBP or *Mycobacterium tuberculosis* PstS-1 structures were carried out using *LSQMAN* from the Uppsala Software Factory *DEJAVU* package (Kleywegt, 1996). The same program was used to calculate the root-mean-square deviation (r.m.s.d.) values. All figures depicting structures were prepared using *PyMOL* (DeLano, 2002).

3. Results

3.1. Crystallization of the target proteins

Crystals of OppA, PstS, PiuA, YrbD and CysP were obtained with diffraction limits of 1.6, 2.0, 2.8, 2.8 and 5.0 Å, respectively (Fig. 1, Table 1). It was not possible to deduce the space group of the CysP crystals from the low-resolution data obtained. The relatively high R_{sym} values for PiuA appear to be a consequence of radiation damage. Some low-resolution data were not fully collected for the high-resolution OppA data set, which resulted in a low level of data completion of 87.4%.

3.2. Overall structure of *Y. pestis* OppA

The structure of OppA was solved at 2.0 Å resolution (Fig. 2*a*) by molecular replacement using coordinates from the *S. typhimurium* OppA crystal structure (PDB code 2olb; Tame *et al.*, 1995). Refinement statistics are summarized in Table 2, indicating a final R_{work} value of 21.0% with an R_{free} value of 23.9% for data refined to 2.0 Å resolution (Table 2). The Ramachandran plot showed 88.7% of the OppA residues to be in the most favourable regions, with the remaining 11.3% in the additional allowed regions. A pairwise alignment between the *Y. pestis* and *S. typhimurium* OppA protein sequences (Parkill *et al.*, 2001; Hogarth & Higgins, 1983) is shown in Fig. 2(*b*), indicating that the residues involved in substrate binding are completely conserved. The sequence identity and similarity between these two proteins are 79% and 85%, respectively. A trilysine peptide is present in the substrate-binding site of this structure (Figs. 2*a* and 3), forming interactions with residues Glu32, Val34, Tyr109, Asn246, Asn247, Arg404, His405, Arg413, Ala415, Trp416, Cys417, Asp419 and Thr438. The trilysine is bound in a similar manner in the *Y. pestis* OppA as that observed in the analogous crystal structure of *S. typhimurium* OppA (Tame *et al.*, 1995), with the peptide being completely

enclosed in the protein interior. Tame *et al.* (1994) pointed out that this mode of binding normally imposes high specificity, with the protein fulfilling the hydrogen-bonding requirements and accommodating the trilysine peptide side chains in voluminous hydrated cavities. The high degree of similarity between the *Y. pestis* and *S. typhimurium* OppA protein structures (Fig. 2*c*), both in the overall fold and substrate-binding site (r.m.s.d. of 0.49 Å for 517 C^{α} atoms), suggests that *Y. pestis* OppA also has the capacity to accept a wide range of peptides with varying affinities, as observed for the *S. typhimurium* protein (Sleigh *et al.*, 1999), and can include cell-wall peptides that contain γ-linked and D-amino acids (Goodell & Higgins, 1987).

3.3. Overall structure of *Y. pestis* PstS

The crystal structure of *Y. pestis* PstS (Fig. 4*a*) was solved at 2.0 Å resolution by molecular replacement using coordinates from the crystal structure of the *E. coli* PBP (PDB code 2abh; Luecke & Quiocho, 1990). The sequence identity and similarity between the *Y. pestis* PstS and *E. coli* PBP amino-acid sequences (Parkhill *et al.*, 2001; Surin *et al.*, 1984; Magota *et al.*, 1984) are 86% and 94%, respectively. Refinement statistics are summarized in Table 2, indicating a final $R_{\rm work}$ value of 17.9% with an $R_{\rm free}$ value of 21.6% for data refined to 2.0 Å resolution (Table 2). The Ramachandran plot showed 93.1% of all residues to be in the most favourable region, with the remaining 6.9% in the additional allowed regions. A pairwise alignment of the sequences of *Y. pestis* PstS, *E. coli* PBP and the other structurally characterized related protein PstS-1 from *M. tuberculosis* is shown in Fig. 4(*b*), highlighting the residues involved in phosphate binding. The sequence identity and similarity between the *Y. pestis* PstS and *M. tuberculosis* PstS-1 amino-acid sequences (Parkhill *et al.*, 2001; Braibant *et al.*, 1996) are 33% and 56%, respectively. The protein fold exhibits the characteristic bilobed structure of PBPs, with the pocket for phosphate in the centre of the structure located between the interface of the two domains (Figs. 4*a* and 5). The overall structure is highly similar to the crystal structures of PBP from *E. coli* (r.m.s.d. of 0.52 Å for 321 C^{α} atoms) and PstS-1 from *M. tuberculosis* (PDB code 1pc3; Vyas *et al.*, 2003; r.m.s.d. of 1.48 Å for 321 C^{α} atoms). It was previously observed that the phosphate-binding site of the *E. coli* PBP contains only one Asp residue, Asp56 (Luecke & Quiocho, 1990), while two Asp residues, Asp83 and Asp168, are present in *M. tuberculosis* PstS-1 (Vyas *et al.*, 2003). This led to the suggestion that the *M. tuberculosis* PstS-1 protein will preferentially bind the monobasic form of P_i whereas the *E. coli* protein would favour binding the dibasic form. However, experimental binding studies showed little difference in the measured affinities of monobasic and dibasic phosphate for either of these proteins (Wang *et al.*, 1984),

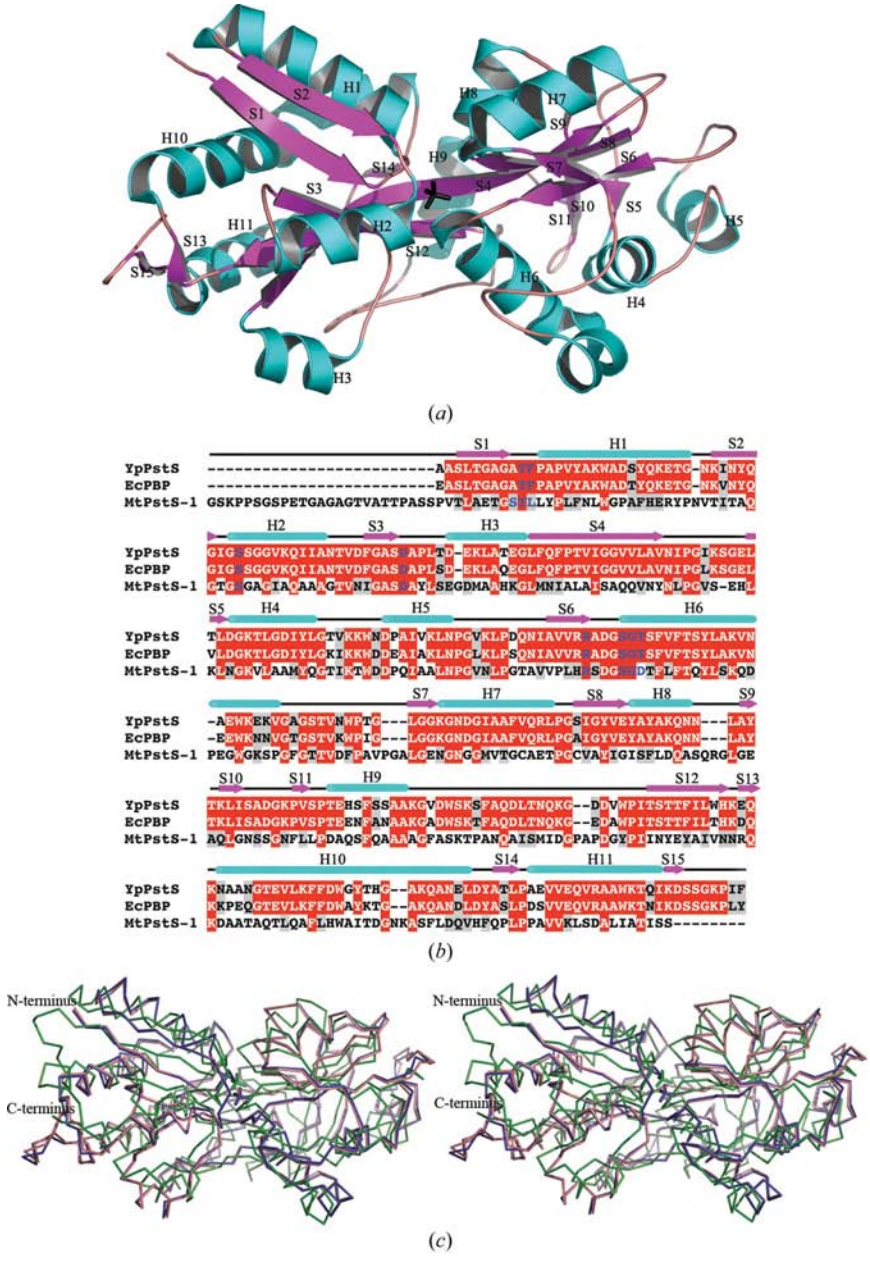

Figure 4
(*a*) Ribbon representation of *Y. pestis* PstS. β-Strands are labelled S1–S15 (purple) and helices are labelled H1–H11 (light blue). The bound phosphate is represented by a stick model. (*b*) The sequences of *Y. pestis* PstS (YpPstS), *E. coli* PBP (EcPBP) and *M. tuberculosis* PstS-1 (MtPstS-1) were aligned using *CLUSTALW* (Thompson *et al.*, 1994). Strands and helices are indicated by purple arrows and light-blue cylinders, respectively. Conserved residues, nonconserved residues and the residues involved in substrate binding are shown in white, black and blue, respectively. (*c*) Parallel stereoview of the superposition of the *Y. pestis* PstS (pink), *E. coli* PBP (dark blue) and *M. tuberculosis* PstS-1 (green) structures.

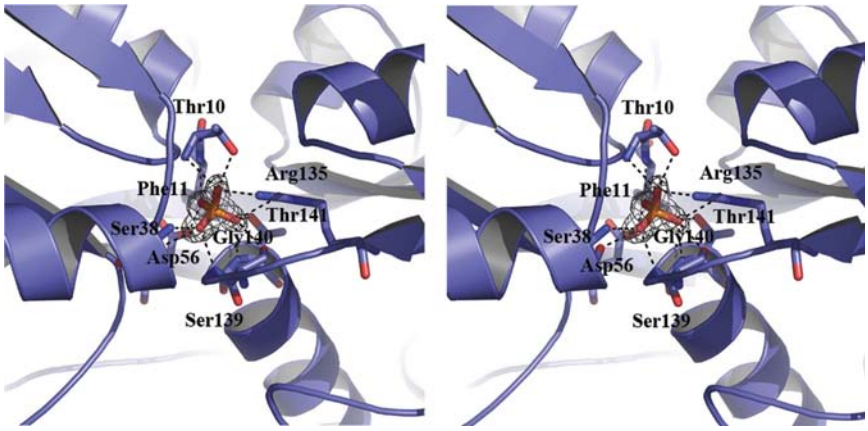

Figure 5
Substrate-binding site of *Y. pestis* PstS shown in parallel stereo. Key binding-site residues are labelled. Electron density for the HPO_4^{2-} is shown generated from a $2F_o - F_c$ difference electron-density map contoured at 1σ. Hydrogen bonds between PstS and HPO_4^{2-} are shown as dotted lines.

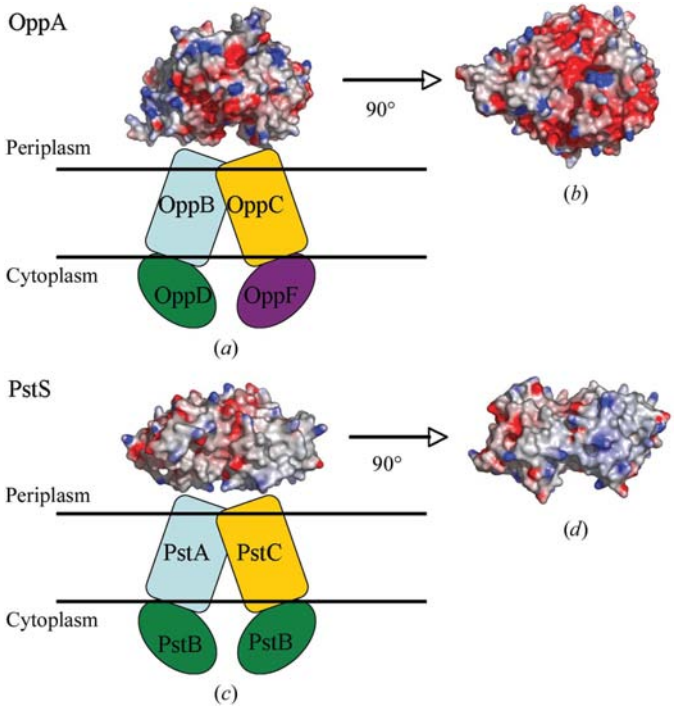

Figure 6
(*a*) Surface model and electrostatic potential map of OppA, shown as if bound to the TMDs. The TMDs (OppB, OppC) and the NBDs (OppD, OppF) are shown as a schematic viewed parallel to the membrane. (*b*) OppA rotated through 90° to show the surface of the protein which will bind to the TMDs. (*c*) Electrostatic potential map of PstS, shown as if bound to the TMDs. The TMDs (PstA, PstC) and NBDs (PstB) are shown as a schematic viewed parallel to the membrane. (*d*) The electrostatic potential map of PstS rotated through 90° to show the surface of the protein which will bind to the TMDs. The surface is coloured according to the electrostatic potential calculated by *GRASP* (Honig & Nicholls, 1995). The polar surfaces are coloured blue (positively charged) and red (negatively charged ($\pm 15kT$/e).

which led to the conclusion that these proteins can transport both substrates (Vyas *et al.*, 2003). The *Y. pestis* PstS binding site (Fig. 5) has only one Asp residue, Asp56, in its binding site, with the position of the second Asp in *M. tuberculosis* PstS-1 being replaced with Thr141, as seen in *E. coli* PBP. *Y. pestis* PstS may thus serve to function in the transport of both P_i species as part of a survival mechanism under conditions of limiting P_i concentration, where it has been shown, for example in *E. coli* and *Bacillus subtilis*, that expression of PstS is highly upregulated (Wanner, 1996; Antelmann *et al.*, 2000). Versatility of substrate binding is also observed in other PBPs such as HisJ, the PBP of the histidine permease ABC transporter from *E. coli*, which also binds arginine, lysine and ornithine although with lower affinity than histidine (Lever, 1972), and, as the name suggests, the leucine-, isoleucine- and valine-binding protein LIVBP (Sack *et al.*, 1989). In addition, the versatility of OppA, which can bind peptides that vary widely in both length and composition, has been well documented (Doeven *et al.*, 2004; Sleigh *et al.*, 1999).

3.4. Structural similarites to other periplasmic binding proteins

The OppA and PstS structures are both comprised of two lobes held together by two and three strands, respectively. This bilobed structure is a common feature of PBPs (Hollenstein *et al.*, 2007; Oh *et al.*, 1994; Quiocho & Ledvina, 1996; Quiocho, 1990). Liganded and unliganded structures of PBPs revealed that the hinge region between the two lobes allows the movement of one lobe relative to the other, with the binding site located in the crevice between the two lobes (Oh *et al.*, 1993; Magnusson *et al.*, 2004; Heddle *et al.*, 2003). This is a conformational rearrangement that appears to be of key importance for high-affinity substrate binding. However, this architecture also has a role in the interaction between the periplasmic binding proteins and the transmembrane-domain regions of the ABC transporter. The recent structure of ModABC indicates that the binding of both lobes to the two TMDs orientates the binding pocket over the translocation pathway (Hollenstein *et al.*, 2007). The interaction between the ModA periplasmic binding protein and the ModB TMDs orientates the entrance of the ModA binding cleft over the ModB gate to the translocation channel. This interaction is suggested to be mediated in part by several charged residues located on the surface of both lobes of ModA. Previous biochemical and mutagenesis studies on HisJ from *S. typhimurium* and FhuD2, an iron-binding protein from *Staphylococcus aureus*, had shown a role for charged residues in the interaction between the relevant PBPs and TMDs. Mutation of key residues on the PBPs resulted in a loss of binding (Liu *et al.*, 1999; Prossnitz, 1991; Sebulsky *et al.*, 2003). A similar mode of interaction was suggested for the components of the vitamin B_{12} ABC transporter BtuF and BtuCD based on the individual structures (Borths *et al.*, 2002) of the proteins. The structure of

the nickel-binding protein NikA from *E. coli* (Heddle *et al.*, 2003; PDB code 1uiv) also appears to have charged amino-acid residues projecting from the protein in the regions likely to interact with the TMDs, although these are not as prominent as in other PBPs. Examination of the surfaces of OppA and PstS predicted to interact with their cognate TMDs shows distinctly different distributions of surface charge (Fig. 6). In the case of PstS (Figs. 6*c* and 6*d*), a number of prominent charged residues are found in positions, previously identified other PBPs (Prossnitz, 1991; Liu *et al.*, 1999; Borths *et al.*, 2002; Sebulsky *et al.*, 2003; Heddle *et al.*, 2003; Hollenstein *et al.*, 2007), as important for interacting with TMDs. This observation suggests that electrostatic interactions play an important role in mediating contacts between PstS and its associated TMDs PstCA. In contrast the OppA structure lacks a considerable number of the charged residues at the equivalent positions in its structure (Figs. 6*a* and 6*b*). This is also the case for the zinc-binding protein ZnuA from *E. coli* (Chandra *et al.*, 2007; PDB code 2ogw), which appears to lack any distinct charged residues on the regions of the protein that are likely to interact with the TMDs. Therefore, whilst it seems likely that electrostatic interactions are of key importance for the association between some PBPs and their specific TMDs, for OppA and possibly other PBPs it is likely that other interactions involving van der Waals forces and hydrogen bonds are also important.

4. Conclusions

The structures of OppA and PstS presented here provide the first examples of ABC transporters from *Y. pestis*. Our initial interest stemmed from previous work which demonstrated that immunization with OppA provides protection against *Y. pestis* infection in a mouse model (Tanabe *et al.*, 2006). This is strongly suggestive that OppA, a protein that is not found in humans, is essential to *Y. pestis* and is therefore a good target for vaccine development. The availability of the three-dimensional structure of OppA provides a framework for the identification and characterization of key epitopes potentially useful for future vaccine development. Furthermore, analyses of both structures indicated that they exhibit a versatility of substrate binding which contributes to the ability of *Y. pestis* to survive, particularly in different niches or under different environmental stresses. Comparisons of surfaces of these proteins also suggest that protein–protein interactions between these PBPs and their cognate TMDs are mediated by a range of molecular forces which are not necessarily dominated by electrostatic interactions as seen in the recent ModABC structure (Hollenstein *et al.*, 2007). Given the wide range of ABC systems which will be functioning in an organism and the similarity of PBP structures in general, these surface differences are clearly key features in assuring correct discrimination and recognition between each PBP and its TMD.

This work was funded by the Defence Science and Technology Laboratories.

References

Antelmann, H., Scharf, C. & Hecker, M. (2000). *J. Bacteriol.* **182**, 4478–4490.

Borths, E. L., Locher, K. P., Lee, A. T. & Rees, D. C. (2002). *Proc. Natl Acad. Sci. USA*, **99**, 16642–16647.

Braibant, M., Lefevre, P., de Wit, L., Peirs, P., Ooms, J., Huygen, K., Andersen, A. B. & Content, J. (1996). *Gene*, **176**, 171–176.

Brown, J. S., Ogunniyi, A. D., Woodrow, M. C., Holden, D. W. & Paton, J. C. (2001). *Infect. Immun.* **69**, 6702–6706.

Brünger, A. T., Adams, P. D., Clore, G. M., DeLano, W. L., Gros, P., Grosse-Kunstleve, R. W., Jiang, J.-S., Kuszewski, J., Nilges, M., Pannu, N. S., Read, R. J., Rice, L. M., Simonson, T. & Warren, G. L. (1998). *Acta Cryst.* D**54**, 905–921.

Chandra, B. R., Yogavel, M. & Sharma, A. (2007). *J. Mol. Biol.* **367**, 970–982.

Collaborative Computational Project, Number 4 (1994). *Acta Cryst.* D**50**, 760–763.

Davidson, A. L. & Chen, J. (2004). *Annu. Rev. Biochem.* **73**, 241–268.

Dawson, R. J. & Locher, K. P. (2006). *Nature (London)*, **443**, 180–185.

DeLano, W. L. (2002). *PyMOL.* http://www.pymol.org.

Detmers, F. J., Lanfermeijer, F. C. & Poolman, B. (2001). *Res. Microbiol.* **152**, 245–258.

Doeven, M. K., Abele, R., Tampe, R. & Poolman, B. (2004). *J. Biol. Chem.* **279**, 32301–32307.

Garmory, H. S. & Titball, R. W. (2004). *Infect. Immun.* **72**, 6757–6763.

Goodell, E. W. & Higgins, C. F. (1987). *J. Bacteriol.* **169**, 3861–3865.

Goosen, N. & Moolenaar, G. F. (2001). *Res. Microbiol.* **152**, 401–409.

Guyer, C. A., Morgan, D. G., Osheroff, N. & Staros, J. V. (1985). *J. Biol. Chem.* **260**, 10812–10818.

Hantke, K. (2005). *Curr. Opin. Microbiol.* **8**, 196–202.

Heddle, J., Scott, D. J., Unzai, S., Park, S.-Y. & Tame, J. R. H. (2003). *J. Biol. Chem.* **278**, 50322–50329.

Higgins, C. F. (1992). *Annu. Rev. Cell Biol.* **8**, 67–113.

Hogarth, B. G. & Higgins, C. F. (1983). *J. Bacteriol.* **153**, 1548–1551.

Hollenstein, K., Frei, D. C. & Locher, K. P. (2007). *Nature (London)*, **446**, 213–216.

Honig, B. & Nicholls, A. (1995). *Science*, **268**, 1144–1149.

Inglesby, T. V. *et al.* (2002). *JAMA*, **283**, 2281–2290.

Jones, T. A., Zou, J.-Y., Cowan, S. W. & Kjeldgaard, M. (1991). *Acta Cryst.* A**47**, 110–119.

Kleywegt, G. J. (1996). *Acta Cryst.* D**52**, 842–857.

Koster, W. (2005). *Front. Biosci.* **10**, 462–477.

Krogh, A., Larsson, B., von Heijne, G. & Sonnhammer, E. L. (2001). *J. Mol. Biol.* **305**, 567–580.

Lamzin, V. S., Perrakis, A. & Wilson, K. S. (2001). *International Tables for Crystallography*, Vol. *F*, edited by M. Rossmann & E. Arnold, pp. 720–722. Dordrecht: Kluwer Academic Publishers.

Laskowski, R. A., MacArthur, M. W., Moss, D. S. & Thornton, J. M. (1993). *J. Appl. Cryst.* **26**, 283–291.

Lever, J. E. (1972). *J. Biol. Chem.* **247**, 4317–4326.

Liu, C. E., Liu, P. G., Wolf, A., Lin, E. & Ames, G. F. (1999). *J. Biol. Chem.* **274**, 739–747.

Locher, K. P., Lee, A. T. & Rees, D. C. (2002). *Science*, **296**, 1091–1098.

Luecke, H. & Quiocho, F. A. (1990). *Nature (London)*, **347**, 402–406.

Magnusson, U., Salopek-Sondi, B., Luck, L. A. & Mowbray, S. L. (2004). *J. Biol. Chem.* **279**, 8747–8752.

Magota, K., Otsuji, N., Miki, T., Horiuchi, T., Tsunasawa, S., Kondo, J., Sakiyama, F., Amemura, M., Morita, T., Shinagawa, H. & Nagata, A. (1984). *J. Bacteriol.* **157**, 909–917.

Murshudov, G. N., Vagin, A. A. & Dodson, E. J. (1997). *Acta Cryst.* D**53**, 240–255.

Oh, B.-H., Kang, C.-H., De Bondt, H., Kim, S.-H., Nikaido, K., Joshi, A. K. & Ames, G. F. (1994). *J. Biol. Chem.* **269**, 4135–4143.

Oh, B.-H., Pandit, J., Kang, C.-H., Nikaido, K., Gokcen, S., Ames, G. F. & Kim, S.-H. (1993). *J. Biol. Chem.* **268**, 11348–11355.

Otwinowski, Z. & Minor, W. (1997). *Methods Enzymol.* **276**, 307–326.

Parkhill, J. *et al.* (2001). *Nature (London)*, **413**, 523–527.
Perry, R. D. & Fetherston, J. D. (1997). *Clin. Microbiol. Rev.* **10**, 35–66.
Piddock, L. J. (2006). *Nature Rev. Microbiol.* **4**, 629–636.
Pinkett, H. W., Lee, A. T., Lim, P., Locher, K. P. & Rees, D. C. (2007). *Science*, **315**, 373–377.
Prossnitz, E. (1991). *J. Biol. Chem.* **266**, 9673–9677.
Quiocho, F. A. (1990). *Philos. Trans. R. Soc. London Ser. B Biol. Sci.* **326**, 341–351.
Quiocho, F. A. & Ledvina, P. S. (1996). *Mol. Microbiol.* **20**, 17–25.
Sack, J. S., Saper, M. A. & Quiocho, F. A. (1989). *J. Mol. Biol.* **206**, 171–191.
Sambrook, J. & Russell, D. W. (2001). *Molecular Cloning: A Laboratory Manual*, 3rd ed. Cold Spring Harbor, NY, USA: Cold Spring Harbor Laboratory Press.
Schneider, E. (2001). *Res. Microbiol.* **152**, 303–310.
Sebulsky, M. T., Shilton, B. H., Spezialli, C. D. & Heinrichs, D. E. (2003). *J. Biol. Chem.* **278**, 46890–49900.
Sleigh, S. H., Seavers, P. R., Wilkinson, A. J., Ladbury, J. E. & Tame, J. R. (1999). *J. Mol. Biol.* **291**, 393–415.
Storoni, L. C., McCoy, A. J. & Read, R. J. (2004). *Acta Cryst.* D**60**, 432–438.
Surin, B. P., Jans, D. A., Fimmel, A. L., Shaw, D. C., Cox, G. B. & Rosenberg, H. (1984). *J. Bacteriol.* **157**, 772–778.
Tame, J. R., Dodson, E. J., Murshudov, G., Higgins, C. F. & Wilkinson, A. J. (1995). *Structure*, **3**, 1395–1406.
Tame, J. R., Murshudov, G. N., Dodson, E. J., Neil, T. K., Dodson, G. G., Higgins, C. F. & Wilkinson, A. J. (1994). *Science*, **264**, 1578–1581.
Tanabe, M., Atkins, H. S., Harland, D. N., Elvin, S. J., Stagg, A. J., Mirza, O., Titball, R. W., Byrne, B. & Brown, K. A. (2006). *Infect. Immun.* **74**, 3687–3691.
Thompson, J. D., Higgins, D. G. & Gibson, T. J. (1994). *Nucleic Acids Res.* **22**, 4673–4680.
Vagin, A. & Teplyakov, A. (2000). *Acta Cryst.* D**56**, 1622–1624.
Vyas, N. K., Vyas, M. N. & Quiocho, F. A. (2003). *Structure*, **11**, 765–774.
Wang, Z., Choudhary, A., Ledvina, P. S. & Quiocho, F. A. (1984). *J. Biol. Chem.* **269**, 25091–25094.
Wanner, B. L. (1996). *Escherichia coli and Salmonella: Cellular and Molecular Biology*, 2nd ed., edited by F. C. Neidhardt, Vol. 1, pp. 1357–1381. Washington DC: ASM Press.
Yakushi, T., Matsuyama, S. & Tokuda, H. (2000). *Nippon Saikingaku Zasshi*, **55**, 517–526.